THE JOURNAL OF PHYSICAL CHEMISTRY A

 VOLUME 104, NUMBER 50, DECEMBER 21, 2000

ARTICLES

Exploring Single-File Diffusion in One-Dimensional Nanochannels by Laser-Polarized ^{129}Xe NMR Spectroscopy

Thomas Meersmann,[†,‡] John W. Logan,[†] Roberto Simonutti,[†,§] Stefano Caldarelli,[||] Angiolina Comotti,[§] Piero Sozzani,[§] Lana G. Kaiser,[†] and Alexander Pines*[,†]

Materials Sciences Division, Lawrence Berkeley National Laboratory, and Department of Chemistry, University of California, Berkeley, California 94720, Materials Science Department, University of Milano-Bicocca, Via Cozzi 53, I - 20125, Italy, and Institut de Recherches sur la Catalyse - CNRS, 2 avenue Albert Einstein, F - 69626 Villeurbanne CEDEX, France

Received: June 30, 2000; In Final Form: August 24, 2000

Single-file diffusion behavior is expected for atoms and molecules in one-dimensional gas phases of nanochannels with transverse dimensions that do not allow for the particles to bypass each other. Although single-file diffusion may play an important role in a wide range of industrial catalytic, geologic, and biological processes, experimental evidence is scarce despite the fact that the dynamics differ substantially from ordinary diffusion. We demonstrate the application of continuous-flow laser-polarized ^{129}Xe NMR spectroscopy for the study of gas transport into the effectively one-dimensional channels of a microporous material. The novel methodology makes it possible to monitor diffusion over a time scale of tens of seconds, often inaccessible by conventional NMR experiments. The technique can also be applied to systems with very small mobility factors or diffusion constants that are difficult to determine by currently available methods for diffusion measurement. Experiments using xenon in nanochannel systems can distinguish between unidirectional diffusion and single-file diffusion. The experimental observations indicate that single-file behavior for xenon in an organic nanochannel is persistent even at long diffusion times of over tens of seconds. Finally, using continuous-flow laser-polarized ^{129}Xe NMR spectroscopy, we describe an intriguing correlation between the observed NMR line shape of xenon within the nanochannels and the gas transport into these channels.

Introduction

Atoms and molecules in liquids or gases of sufficient density experience random, three-dimensional Brownian motion on the microscopic scale, which leads to macroscopic displacements at longer time scales. A mean displacement of the particles is defined for time scales that are long compared to the time between individual collisions, and its time dependence is described by the well-known Einstein equation

$$\langle x^2(t)\rangle = 2nDt \tag{1}$$

where $n = 1$, 2, or 3 for one-, two-, or three-dimensional diffusion and D is the self-diffusion constant ($[D] = m^2/s$). The Brownian motion on the microscopic scale may still be three-dimensional when the particles are confined within one-dimensional channels even when macroscopic displacement occurs only along the channel axis. In this case, diffusion is

* Corresponding author. E-mail: pines@cchem.berkeley.edu.
[†] Lawrence Berkeley National Laboratory and University of California at Berkeley.
[‡] Permanent address: Department of Chemistry, Colorado State University, Fort Collins, CO 80235. E-mail: meersman@lamar.colosate.edu.
[§] University of Milano-Bicocca.
[||] Institut de Recherches sur la Catalyse.

10.1021/jp002322v CCC: $19.00
Published on Web 11/23/2000

considered to be unidirectional, and pulse field gradient (PFG) NMR measurements will typically register one-dimensional diffusion displaying time dependence as described by eq 1, with $n = 1$. The situation changes when the transverse channel dimensions are about the same size as the atoms or molecules inside the channel. In such systems, the particles can no longer bypass each other, and the microscopic motion cannot be considered as three-dimensional. The resulting diffusion is termed single-file diffusion, and the time dependence of the mean displacement changes to

$$\langle x^2(t)\rangle = 2F\sqrt{t} \qquad (2)$$

where the mobility factor F ($[F] = m^2\sqrt{s}$) is introduced.[1−4] This phenomenon should be rather common in one-dimensional channel systems and has been subjected to theoretical studies in the past.[5−8] Only a few experimental verifications of single-file diffusion have been provided so far using pulse field gradient (PFG) NMR spectroscopy[9−11] at time scales of milliseconds to hundreds of milliseconds and by quasi-elastic neutron scattering[12] with time scales in the microsecond regime. The long-time behavior of gas diffusion over periods relevant, for instance, in catalytic processes has been experimentally inaccessible thus far. In this contribution, we demonstrate a persistence of single-file diffusion behavior over tens of seconds for the one-dimensional gas phase in ca. 500 pm diameter nanochannels of tris(*o*-phenylenedioxi)cyclophosphazene (TPP). The technique applied for the study of this system utilizes continuous-flow laser-polarized ^{129}Xe NMR spectroscopy and differs drastically from conventional diffusion measurements.

Experimental Section

Circular polarized light from a 100 W diode array laser (Opto Power Corp.) was used for optical pumping at the D_1 transition of rubidium (794.7 nm) within a Pyrex pumping cell containing a small amount of rubidium vapor and xenon−helium gas mixture.[13,14] The gas was pressurized at about 800 kPa and temperatures of 400−450 K, and mixtures containing 2.5% xenon, 30% xenon, or pure xenon (natural isotopic abundance, 26.4% ^{129}Xe) were used for the optical pumping experiments. Spin exchange during gas-phase collisions between rubidium and ^{129}Xe atoms results in a xenon nonequilibrium nuclear spin polarization of ca. 1−10% (depending on the gas mixture). The spin polarization is defined as $p = |n_\uparrow - n_\downarrow|/(n_\uparrow + n_\downarrow)$, with $n_\uparrow$ and $n_\downarrow$ as the populations of the energy levels. At 300 K and 11.75 T, the thermal equilibrium polarization is only $p = 0.0011\%$. A 1% polarization at 11.75 T in thermal equilibrium would require a temperature of 0.33 K; hence, laser-polarized xenon can be thought to be at extremely low spin temperatures and is represented by blue shading in the sketches in Figure 1. Thermally polarized xenon at all magnetic field strengths and xenon depolarized by radio frequency pulses are symbolized by red shading. Xenon marked by red shading is not observable at the experimental conditions described here, where only laser-polarized xenon at low spin temperature, far from a thermal equilibrium state, gives rise to observable signals.

After spin exchange with rubidium and being passed through the pumping cell, the xenon gas is expanded to atmospheric pressure and transferred into the high magnetic field region (11.75 T). It flows via a glass capillary into a 7.5 mm magic-angle spinning (MAS) NMR probe for detection (see Figure 1A). The ^{129}Xe spectra were obtained using a 500 MHz Chemagnetics Infinity spectrometer operating at 138.33 MHz for ^{129}Xe. Nitrogen gas is usually added to the optical pumping mixture as a radiation trap in order to increase the efficiency of the xenon laser polarization. However, it was omitted in our experiments to avoid interference with the diffusion measurements. Helium was assumed not to alter the single-file diffusion behavior of xenon and provided a simple way to alter xenon concentration in the detection cell.

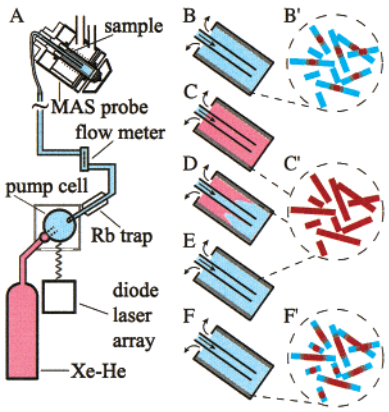

Figure 1. (A) Basic setup of the experiment. Xe−helium gas mixtures, at thermal polarization (red), are pumped into a cell irradiated with circularly polarized laser light. The laser-polarized xenon gas passes through a water condenser to remove the gas-phase Rb and continues into the probe head. (B and closeup B′) Sample cell after infinite flow of polarized xenon. The laser-polarized gas (blue) penetrates the crystallites, likely relaxing to thermal polarization prior to diffusing into the center of the crystallites. (C and closeup C′) Sample cell immediately after saturation train. The xenon polarization inside the sample region is destroyed. (D−F, and closeup F′) Cell after increasing times τ. The flow of new polarized xenon flows into the sample region and diffuses into the crystallites.

Sample spinning at 5 kHz for about 30 min has been used to prepare a thin layer (few hundred microns) of TPP crystallites on the spinner wall, thus reducing the influence of gas diffusion through the crystallite powder. All experiments for the study of single-file diffusion were performed under static (i.e., nonspinning) conditions. Figure 2C shows an actual static spectrum of xenon with a gas-phase signal at 0 ppm, and a signal with strong chemical shift anisotropy at about 100 ppm arises from xenon inside the nanochannels. Figure 2D displays the 2 kHz MAS spectrum recorded under otherwise identical conditions.

The basic TPP building block is depicted in Figure 2A, and the channel structure becomes apparent from Figure 2B. The synthesis of the TPP/benzene inclusion compound was performed as previously reported by Allcock,[15] and the pseudohexagonal modification of TPP with the empty channel structure was obtained by evacuation (10^{-2} Torr) at 343 K.[16] The fitting of the CSA patterns was performed using variables δ_{iso}, $\Delta\delta$, η, and the line width with the following definitions: $|\delta_{33} - \delta_{iso}| > |\delta_{11} - \delta_{iso}| > |\delta_{22} - \delta_{iso}|$, $\delta_{iso} = (\delta_{11} + \delta_{22} + \delta_{33})/3$, $\Delta\delta = \delta_{33} - \delta_{iso}$, and $\eta = (\delta_{22} - \delta_{11})/(\delta_{33} - \delta_{iso})$.

Monitoring Gas Transport

Figures 1B and 1B′ show a closeup of the sample region. Polarized xenon enters the MAS spinner through a capillary (blue) where it continues to diffuse into the nanochannels of the crystallites (bars). Smaller crystallites are completely filled with polarized xenon (blue). However, the laser-polarized xenon may relax during diffusion into the nanochannels and may reach the center of longer crystallites only as thermally polarized xenon (red) that can no longer be detected in our experiment.

The actual measurement of xenon gas transport into the nanochannels starts with a train of 90° saturation pulses that

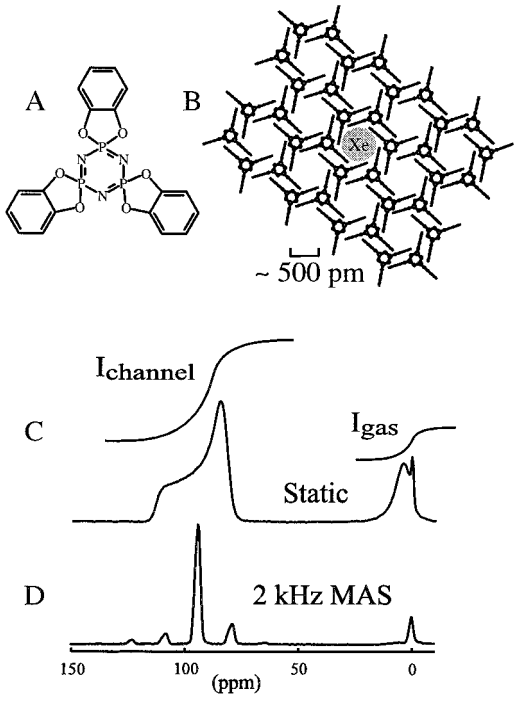

Figure 2. (A) Basic building block of TPP crystallites. (B) The nanochannels are composed of stacked prisms with a triangular base, where the benzene rings of TPP are the vertical faces. Neighboring prisms are rotated by 60° along the vertical axis, resulting in hexagonal channels that can be considered with good approximation as cylinders of 500 pm diameter. The π electrons of the benzene units are facing the interior of the channel and are in close proximity to the 1-D gas-phase xenon guest atoms. (C) Continuous-flow optical pumping ^{129}Xe NMR spectrum for xenon in contact with TPP at 273 K and a buildup time of 10 s. The signal from xenon inside the nanochannel is shifted at around 90 ppm with reference to the gas-phase peak at 0 ppm. The broad peak overlapping with the gas-phase transition is most likely from xenon in the vicinity and between the crystallites, where it is in close contact with the outer surface of the TPP. The intensity of this peak does not change substantially with temperature. (D) A 2 kHz MAS spectrum taken under conditions otherwise identical to those in C.

destroys all xenon polarization within the detection cell (Figure 1C). Since the experiments are performed under continuous-flow conditions, the nonpolarized xenon is immediately replaced with laser-polarized xenon (Figure 1D). The gas phase is completely exchanged with laser-polarized xenon after approximately 50−200 ms (depending on the flow rate), as shown in Figure 1E. This step can be verified experimentally by monitoring the signal intensity from the gas-phase xenon. The saturation train is followed by a buildup time delay τ and signal acquisition after the final excitation pulse (Figure 1C′). The amount of laser-polarized xenon inside the channels (see Figure 1F′) will increase with increasing time τ until all channels are filled or a steady state due to longitudinal relaxation inside the material has been reached (see again Figures 1B and 1B′).

In this contribution, it is demonstrated how the methodology recently introduced for the imaging of flow and diffusion into porous materials[17] can be applied in order to distinguish between ordinary diffusion and single-file diffusion. The method is analogous to previous measurements of the diffusion of light water into a gel made with heavy water[18] and is based on the time dependence of the ^{129}Xe signal inside the channels which reflects the total gas transport into the porous material. The technique follows quite naturally from the experimental setup of continuous-flow laser-polarized ^{129}Xe NMR and can therefore easily be implemented. Figure 3 provides a sketch of the basic idea. In Figure 3A, polarized xenon diffuses into nanochannels

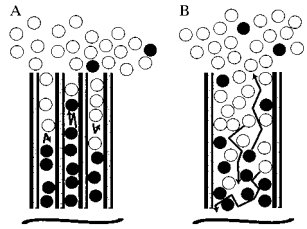

Figure 3. Sketches of gas particles diffusing in a channels. (A) The channel is only slightly larger than the gas particles, leading to single-file diffusion and causing a time dependence in the signal intensities described by eq 4. (B) A channel with a diameter somewhat larger than the diameter of the gas particles will most likely lead to unidirectional (i.e., ordinary) diffusion with the time dependence described by eq 3.

with diameters only slightly larger than the xenon diameter of 440 pm. In contrast, Figure 3B depicts a hypothetical channel with a transverse dimension much larger than the xenon diameter. The saturation train will destroy the laser-enhanced xenon polarization, and the detected signal is solely due to laser-polarized xenon subsequently entering the detection cell and diffusing into the channels. The signal intensity is a direct function of the mean free pathway of the xenon into the channels with a time dependence described by either eq 1 or eq 2, depending on the channel diameter.

The measurement of the xenon uptake inside the nanochannels is meaningful only after the gas phase in the entire sample region has been replaced by polarized xenon via flow and diffusion through the thin layer of TPP powder. During the initial "dead-time" of ca. 50−200 ms, the polarized xenon is not in contact with all of the crystallites, and some error will arise from the uncertainties during the initial 50−200 ms. Selective irradiation of the xenon−nanochannel transition during the initial 200 ms after the saturation train could prevent this error but has not produced substantially different results from pulse sequences without selective saturation. Since the xenon line width changes with temperature, the efficiency of the selective saturation may vary with temperature and therefore has not been used for the measurements shown in Figure 4.

Results

Continuous-flow optical pumping ^{129}Xe NMR provides the means to distinguish between unidirectional and single-file diffusion at time scales between a few hundred milliseconds to many tens of seconds. However, longitudinal relaxation will dampen the signal intensity for longer buildup times and has to be taken into account for an expression of the time dependence of the signal intensity. It follows for unidirectional (i.e., ordinary) diffusion that

$$I_{channel}(\tau)/I_{gas} = C^{D}(T, P)\int_0^{\tau}\frac{1}{\sqrt{t}}\exp(-t/T_1)\,dt \qquad (3)$$

or for single-file diffusion

$$I_{channel}(\tau)/I_{gas} = C^{F}(T, P)\int_0^{\tau}\frac{1}{\sqrt[4]{t^3}}\exp(-t/T_1)\,dt \qquad (4)$$

where the temperature- and gas-pressure-dependent prefactors C^D and C^F contain the information about xenon loading of the channels, the total number of channels, the xenon gas density, and the overall gas volume inside the detection cell. In Figure 4, $I_{channel}/I_{gas}$ is the intensity of the xenon signal from the nanochannels normalized by the intensity of the gas-phase

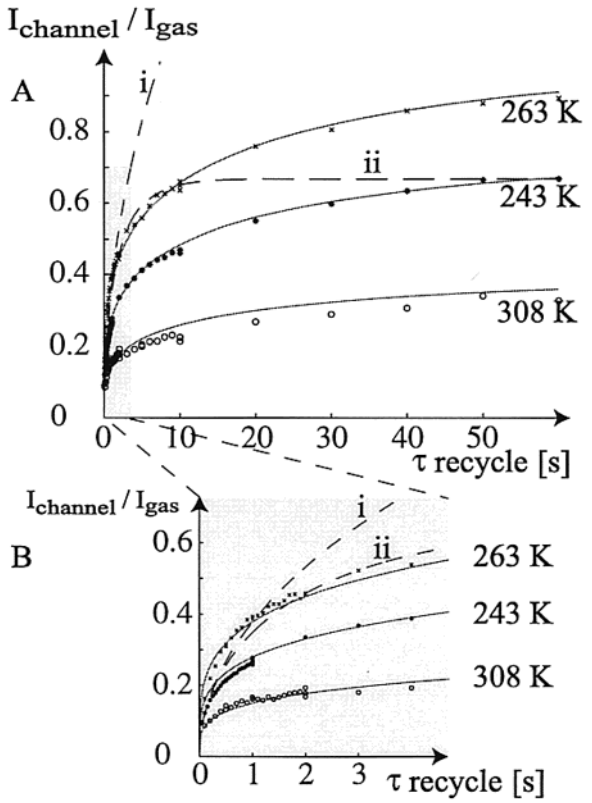

Figure 4. (A) Increase of the integral of the xenon signal over time for three different temperatures (308 K, circles; 243 K, stars; 263 K, crosses). The dashed lines, i and ii, envision the behavior expected from the unidirectional diffusion described by eq 3, with $T_1 = 70$ s for line i and $T_1 = 4$ s for line ii. The solid lines are fits of the experimental data points using eq 4. (B) Expanded view of A.

signal. The normalization takes long-term fluctuations of the optical pumping process into account. The dashed lines in Figure 4 show the behavior that is expected for unidirectional diffusion. Neither for long relaxation times (i.e., $T_1 = 70$ s, line i.) nor for short relaxation times (i.e., $T_1 = 4$ s, line ii.) does eq 3 reflect the experimental buildup curves. The experiments were recorded using a 2.5% xenon in helium mixture at 243, 263, and 308 K. The solid lines are the result of eq 4 and can provide a close fit of the experimental data points. The relaxation time used for the fits at all temperatures is $T_1 = 70$ s. Note, that the T_1 values cannot be measured directly by inversion recovery in continuous-flow optical pumping experiments. The ratio of the prefactor constants for the different temperatures can be obtained by fitting the experimental data with eq 4, yielding C^F(243 K):C^F(263 K):C^F(308 K) = 1.9:2.7:1. The temperature dependence of this constant reflects the changes in the mobility factor F ($[F] = m^2\sqrt{s}$) as well as changes in the xenon loading of the channels.

These data provide the first experimental observation that gas transport in nanochannels exhibits single-file diffusion behavior over pronounced periods of time. The measurement of single-file diffusion over the very long time periods is possible only because the nanochannels can be assumed to be of infinite length compared to the mean displacement of the xenon atoms during the time scales observed. The uptake curve reaches maximum intensity plateaus after approximately 180 s, which is most likely caused by relaxation rather than by completely filling the channels with polarized xenon.

Correlation of the Xenon Transport into the Nanochannels with the Xenon Line Shape. The buildup curves at three different temperatures reveal an interesting behavior of the constant $C^F(T)$, which exhibits its largest value at the intermediate temperature of 243 K. Instead of mapping $C^F(T)$, which would require very long experimental times and high xenon usage for the open flow system, we can compare the signal intensity for various temperatures at one particular time of the xenon uptake. Figure 5A displays the intensities of the xenon signal inside the nanochannels after a $\tau = 10$ s buildup as a function of temperature for three different xenon concentrations. The signal intensity increases as the temperature is lowered and goes through a maximum at a temperature value that depends on the xenon concentration. Further reduction in temperature leads to decreasing signal intensity. Note that a temperature-dependent change in the channel geometry does not provide an explanation for this behavior, since it cannot account for the observed temperature shift of the curves for different xenon concentrations.

A temperature and gas concentration dependence can also be seen in the xenon chemical shift anisotropy (CSA) (see Figures 2C,D and 5B). An anisotropic line shape cannot be usually observed for xenon in systems with three-dimensional porous networks. All observations of xenon CSA in porous materials so far were restricted to systems containing one-dimensional channels with transverse dimensions similar to the xenon radius.[19−21] However, the one-dimensional channels used in their experiments (e.g., aluminum phosphate molecular sieves) do not possess a cylindrical symmetry like that of the TPP nanochannels for which the xenon CSA pattern shows a nearly perfect axial symmetry.[22] Figure 5B shows that the axially symmetric ^{129}Xe CSA at 293 K collapses to an isotropic peak as the concentration of the gas is increased from 2.5% to 30% xenon and the anisotropy reoccurs with an inverted sign for pure xenon at the same temperature. (The overall pressure was kept at about 100 kPa for all experiments shown in Figure 5.) In addition, Figure 5B also demonstrates the temperature dependence of the xenon CSA. The positive anisotropy at 293 K and 2.5% xenon is reduced with decreasing temperature, and at about 243 K, the transition becomes isotropic. Further decrease in temperature leads to a line shape with negative anisotropy. The line shapes show comparable temperature dependence for all gas mixtures except for a shift to higher overall temperature values with increasing concentration.

Xenon atoms that are mainly affected by van der Waals interactions with the π electrons of the channel walls can explain the observed xenon line shape at low xenon concentrations and high temperatures. This will lead to a CSA with positive and axially symmetric anisotropy. As concentration or pressure is increased or, alternatively, as the temperature is lowered, the xenon loading inside the channels rises, and the xenon−xenon distance r_{Xe-Xe} decreases. This may cause a dramatic increase in the xenon−xenon interactions due to the $1/r_{Xe-Xe}^6$ dependence of the van der Waals forces. At the onset of the xenon−xenon interactions at low loadings, the positive anisotropy will first be reduced and subsequently collapsed to an isotropic line shape before the xenon−xenon interactions become dominant over xenon−wall interactions at very high loadings, resulting in an axially symmetric CSA with negative anisotropy.

A comparison of panels A and B of Figure 5 reveals that there is an intriguing correlation between the temperature dependence of the signal intensity and the temperature dependence of the line shape. An isotropic ^{129}Xe line shape (heavy lines in panel B and dashed lines in panel A) in the nanochannels is observable at about 15−20 K below the temperature that leads to the maximum observable xenon/TPP−channel signal (solid lines in panel A). This correlation can be seen consistently at

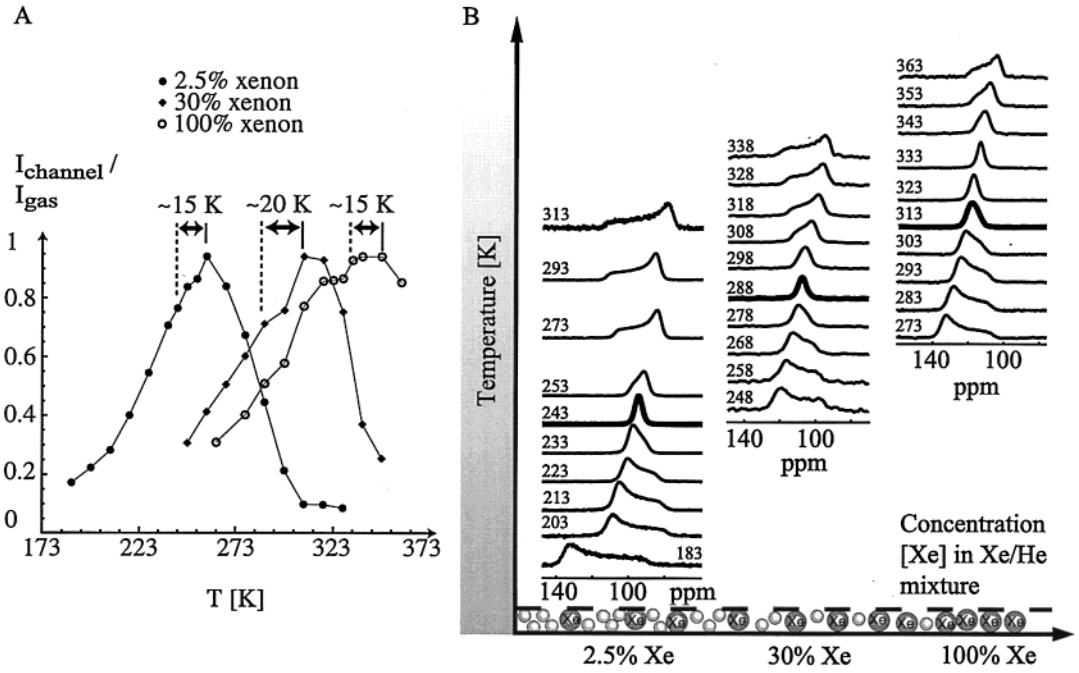

Figure 5. (A) Experimental signal intensities (integrated) in continuous-flow optical pumping ^{129}Xe NMR for xenon inside the TPP channels as function of temperature for three different concentrations, i.e., 2.5% (filled circles), 30% (filled diamonds), and 100% (open circles). The buildup time was 10 s. Lines mark maximum intensity (solid line) and isotropic transition (dashed line, heavy line in B). (B) Continuous-flow optical pumping ^{129}Xe NMR line shapes for xenon inside TPP channels at various temperatures and three different concentrations: 2.5% xenon in helium, 30% xenon in helium, and 100% xenon, all at atmospheric pressure (100 kPa). The xenon−helium mixture is kept at a constant pressure of 100 kPa for all experiments. The fitting of the line shape resulted in a CSA tensor values of $\eta = 0$.[a] [[a] Footnoted table:] other fitting parameters for various gas mixture/temperature combinations. Instead of an alteration in the xenon concentration (i.e., the partial pressure of the xenon), variations in the overall pressure of pure xenon gas lead again to similar changes in the line shape (not depicted).

Xe conc. / Temperature [K]	δ_{iso} [ppm]	$\Delta\delta$ [ppm]
2.5% / 293	92.3	16.6
2.5% / 243	95.3	2.3
2.5% / 203	102.3	–21.0
30% / 288	106.4	2.5
100% / 333	114.0	3.2

all xenon concentrations despite the overall temperature shift of 90 K for the various xenon−helium mixtures.

To explain this correlation, we must consider that the heterogeneous xenon−nanochannel system in the NMR detection cell is in a thermodynamic equilibrium state (except for the spin polarization) and that channel loading will increase with decreasing temperature or with increasing xenon gas concentration. The transport of the laser-polarized xenon into the channels depends on the diffusion within the nanochannels and is therefore kinetically controlled. However, single-file diffusion depends strongly on the channel loading

$$F = \sqrt{\frac{D_0}{\pi}}\sigma\frac{(1-\theta)}{\theta} \qquad (5)$$

where D_0 is the theoretical (temperature dependent) diffusion constant of a single xenon atom in the channel, σ is the radius of the xenon atom, and θ is the loading of the channel in this "hard-sphere approach".[8] The mobility factor F should therefore decrease with decreasing temperature partially due to the increased loading of the TPP nanochannels and partially due to the smaller diffusion constant D_0. Despite the reduced diffusion, the signal may still gain in intensity by lowering the temperature because of the increased xenon loading and therefore higher number of spins inside the channels. As the temperature is further reduced, the loading will approach a high filling factor with limited possibilities for additional loading increase. The reduced diffusion lowers the signal intensity as the temperature continues to decrease. The turning point in the temperature

dependence of the xenon signal intensity will be accompanied by substantial xenon−xenon interactions inside the channel and will therefore be reflected in the observed xenon line shape. For TPP, the maximum intensity is reached at about 15 K before the isotropic line shape is observed, independent of the used xenon concentration. Higher xenon gas-phase concentration will lead to larger xenon loading for a given temperature, and the temperature-intensity curves are therefore shifted to higher temperatures. In addition to the thermodynamics and kinetics inside the nanochannels, the xenon signal intensities may also be influenced by the rate of exchange from the pure gas phase into the channels (i.e., at the channel openings). However, the correlation between the temperature dependencies of the ^{129}Xe signal intensity with its line shape seems to exclude this possibility, since the line shape is generated only inside a channel. This evidence provides a strong indication that exchange processes do not determine the rate of the signal uptake, at least for the time scales used in our experiments (many hundreds of milliseconds and beyond).

Conclusions

Continuous-flow optical pumping ^{129}Xe NMR spectroscopy provides a unique tool for distinguishing between one-dimensional and single-file diffusion, particularly concerning their behavior over long time scales on the order of seconds or many tens of seconds. It can also be used when the diffusion constants are too small to be investigated by conventional pulse field gradient NMR. Although the diffusion constant itself cannot be measured directly without very strong gradients, other aspects of gas transport into nanochannels can be investigated with this technique. Complementary isotherm measurements of the xenon−channel loading at all temperatures and xenon gas concentrations would provide access to the temperature and loading dependence of the mobility factor F. Combined with the correlation between line shape and signal buildup, the technique opens up a method of gaining new insight into the nature of the gas transport in porous materials. This technique will be of great interest for heterogeneous catalysis in particular with respect to shape-selective catalysis in restricted geometry, analytical separation methods, and purification processes. It can contribute to a more basic understanding of the mechanisms that rule gas transport into porous catalysts, molecular sieves, porous rocks, or pore-forming transmembrane proteins in biological systems.

Acknowledgment. This work was supported by the Director, Office of Energy Research, Office of Basic Energy Science, Materials Sciences Division of the U.S. Department of Energy under Contract DE-AC03-76SF00098. T.M. thanks the Alexander von Humboldt foundation for a Feodor-Lynen Fellowship. P.S. thanks the Italian Ministry of University and Scientific Research (PRIN program) for financial support.

References and Notes

(1) Levitt, D. G. *Phys. Rev. A* **1973**, *8*, 3050.
(2) Fedders, P. A. *Phys. Rev. B* **1973**, *17*, 40.
(3) Kärger, J.; Petzold, M.; Pfeifer, H.; Ernst, S.; Weitkamp, J. *J. Catal.* **1992**, *136*, 283.
(4) Hahn, K.; Kärger, J. *Phys. Rev. A* **1995**, *28*, 3061.
(5) Sholl, D. S.; Fichthorn, K. A. *Phys. Rev. Lett.* **1997**, *79*, 3569.
(6) Rödenbeck, C.; Kärger, J.; Hahn, K. *Phys. Rev. E* **1997**, *55*, 5697.
(7) Sholl, D. S. *Chem. Eng. J.* **1999**, *74*, 25.
(8) Sholl, D. S.; Lee, C. K. *J. Chem. Phys.* **2000**, *112*, 817.
(9) Gupta, V.; Nivarthi, S. S.; McCormick, A. V.; Davis, H. T. *Chem. Phys. Lett.* **1995**, *247*, 596.
(10) Hahn, K.; Kärger, J.; Kukla, V. *Phys. Rev. Lett.* **1996**, *76*, 2762.
(11) Kukla, V.; Kornatowski, J.; Demuth, D.; Girnus, I.; Pfeifer, H.; Rees, L. V. C.; Schunk, S.; Unger, K. K.; Kärger, J. *Science* **1996**, *272*, 702.
(12) Jobic, H.; Hahn, K.; Kärger, J.; Bée, M.; Tuel, A.; Noack, M.; Girnus, I.; Kearley, G. J. *J. Phys. Chem. A* **1997**, *101*, 5834.
(13) Raftery, D.; Long, H.; Meersmann, T.; Grandinetti, P. J.; Reven, L.; Pines, A. *Phys. Rev. Lett.* **1991**, *66*, 584.
(14) Brunner, E.; Seydoux, R.; Haake, M.; Pines, A.; Reimer, J. A. *J. Magn. Reson.* **1997**, *130*, 145.
(15) Allcock, H. R.; Siegel, L. A. *J. Am. Chem. Soc.* **1964**, *86*, 5140.
(16) Comotti, A.; Simonutti, R.; Stramare, S.; Sozzani, P. *Nanotechnology* **1999**, *10*, 70.
(17) Kaiser, L.; Meersmann, T.; Logan, J. W.; Pines, A. *Proc. Natl. Acad. Sci.* **2000**, *97*, 2414.
(18) Klemm, A.; Müller, H.-P.; Kimmich, R. *Phys. A* **1999**, *266*, 242.
(19) Springuel-Huet, M. A.; Fraissard, J. *Chem. Phys. Lett.* **1989**, *154*, 299.
(20) Ripmeester, J. A.; Ratcliffe, C. I. *J. Phys. Chem.* **1995**, *99*, 619.
(21) Jameson, C. J.; Jameson, A. K.; Gerald, R. E., II.; Lim, H.-M. *J. Phys. Chem. B* **1997**, *101*, 8418.
(22) Sozzani, P.; Comotti, A.; Simonutti, R.; Meersmann, T.; Logan, J. W.; Pines, A. *Angew. Chem., Int. Ed. Engl.* **2000**, *39*, 2695.